Coordinating Backbending to Quadrupedal Locomotion on Flat Ground and Improving Gait Stability with an Inertia Tail

Haosen Xing
Biorobotics Lab
Mechanical Engineering Department
Carnegie Mellon University
Email: haosenx@andrew.cmu.edu

Geometric techniques are used to provide a coordination strategy of body bending to the quadrupedal leg movements. We found that backbending can assist not only in forward motion, but also in turning motion. We verified our results with robot experiments on level ground. Meanwhile, there are two main sequences of footfall patterns for quadrupedal walking: lateral and diagonal, we observed that, compared with the lateral sequence (LS) gait, the diagonal sequence (DS) gait produces a larger stride displacement (i.e., higher average speed), but at the cost of decreased body stability. We aim to increase the stability of the DS gait by investigating the use of an inertial tail-like appendage.

1 Introduction

Coordinating backbending with leg movements has been observed to improve quadrupedal animal's locomotive performance across various substrates [2, 3, 4, 5]. In this work, we demonstrate that backbending has a substantial benefit in quadrupedal locomotion on flat ground. Using a 3D robophysical model (Fig. 1(b)), we verify that proper coordination of backbending increases the stride displacement in forward locomotion and improves turning behavior on level ground.

Geometric mechanics [6, 7, 8, 9] offers powerful tools like connection vector fields and height functions for intuitively analyzing, visualizing and designing locomotor kinematics [10, 11]. It has been applied not only in the study of limbless locomotion [12, 13, 14, 15], but also recently to multi-legged locomotion [16, 17, 1]. Here, we apply geometric techniques to gait motion analysis of quadruped locomotion on level ground.

During the quadrupedal gaits study, as shown in [18], there are two main sequences of footfall patterns for quadrupedal walking: lateral and diagonal. We observed that the LS gait has a smaller stride displacement while maintaining stability, which most quadrupedal animals adopt this gait when walking. On the other hand, the DS gait, most observed in the quadrupedal primates, produces a larger stride displacement but at the cost of stability. In second part of our work, we investigate the use of an inertial tail-like appendage to help stabilize DS gaits for a backbending quadruped robot. With Lagrangian analysis and self-manipulator modeling [19], we can derive desired tail oscillations to keep the DS gait stable.

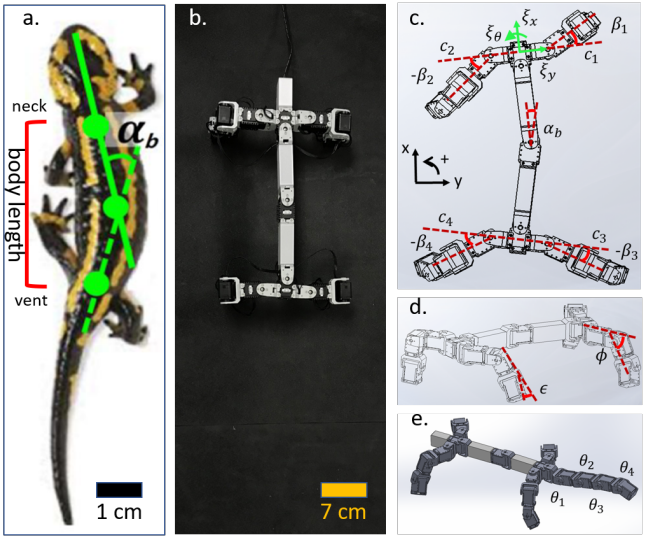

Fig. 1. **The animal, robot and CAD models.** (a) Top view of the fire salamander. Red bracket shows the body length (neck to vent) and body angle α_b measures the angle between first and second body links [1]. (b) top view of the robophysical model. (c)(d) CAD models with relevant joint angles and body velocities labeled. (e) CAD model with tail joints labeled.

2 Background

2.1 Legged Locomotion

Foot placement during legged locomotion has been extensively studied. Methods like footfall planning [20, 21, 22, 23], machine learning [24, 25, 26, 27, 28, 29], biomimet-

ics [30, 31, 32, 33, 34, 35, 36] and central pattern generators (CPGs) [29, 37, 38, 39, 40, 41, 5] have been applied to quadrupedal locomotion. The coordination of backbending and leg movements for quadrupedal locomotion is a comparatively less explored area. [42] introduced a 3D forward dynamics mechanical model of a salamander, using sets of linearly modeled skeletal muscles to generate movements of body and limbs, in order to mimic quadrupedal walking, swimming, and turning. [41] showed that CPGs can produce body-limb coordinated movements, such coordination maximizes the locomotion speed [39, 5] for a trot gait [1]. Their assumption that quadruped locomoting with a trot gait is kinematic stands for the salamander species who keeps tail and part of the trunk in contact with the ground during the whole step cycle. While we observe that most quadrupedal animals locomote on flat ground with only their feet contacting the surface, in which case trot gait is a dynamic gait and out of scope of our work.

Engineers and biologists often assume no-slip contact when modeling legged locomotion. In [43, 44, 45, 46], the foot force distribution was optimized to prevent foot slip. In [47, 48], foot placement was emphasized, and the Little-Dog robot was able to plan a path including selecting footholds that avoid foot slip. In our work, we assume the slip of each foot placement is negligible and there are no linear velocities on all stance feet.

2.2 Geometric Mechanics

This section provides a concise overview of the geometric tools needed for this paper. See [12, 13, 49, 14, 7, 6, 15, 8, 9, 50, 1] for more details.

2.2.1 Kinematic Reconstruction Equation

When analyzing a locomoting system, the configuration space Q can be separated into a position space G and a shape space M, such that the position $g \in G$ locates the system in the world and the shape $r \in M$ describes the relative arrangement of its body. In *principally kinematic systems* [11, 10], we assume its moving is slow enough that momentum is negligible. There exists a linear relationship between changes in the system's shape and changes in its position. In this way, the equation of in-plane motion reduces to

$$\xi = A(r)\dot{r}, \tag{1}$$

where $\xi = [\xi_x\ \xi_y\ \xi_\theta]^T$ denotes the body velocity of the system in forward, lateral and rotational directions, r denotes the shape variables (joint angles), $r \in \mathbb{R}^2$, and the *local connection* $A(r)$ acts as a kind of Jacobian to relate shape velocity $\dot{r}$ to body velocity ξ.

2.2.2 Connection Vector Fields and Height Functions

Each row of $A(r)$ defines a connection vector field in the shape space. Its dot product with the shape velocity $\dot{r}$ is the body velocity. A shape velocity $\dot{r}$ along the direction of the vector field would yield the largest possible body velocity in that direction, while a shape velocity $\dot{r}$ orthogonal to the field would produce zero body velocity.

A *gait* $\partial\phi$ is defined as a cyclic path through the shape space. The net displacement over a gait cycle can be approximated by taking the line integral of the local connection along the closed curve $\partial\phi$ [11, 10, 51]

$$\begin{bmatrix}\Delta x\\ \Delta y\\ \Delta\theta\end{bmatrix} \approx \int_{\partial\phi} A(r)dr, \tag{2}$$

Stokes' Theorem equates this quantity to the surface integral of the curl of $A(r)$ over the area enclosed by $\partial\phi$

$$\int_{\partial\phi} A(r)dr = \iint_{\phi} \nabla \times A(r)dr, \tag{3}$$

where ϕ denotes the area enclosed by $\partial\phi$. The curl of the connection vector field, $\nabla \times A(r)$, is referred to as the *height function*. The three rows of the vector field $A(r)$ can thus produce three height functions in the forward, lateral and rotational direction respectively.

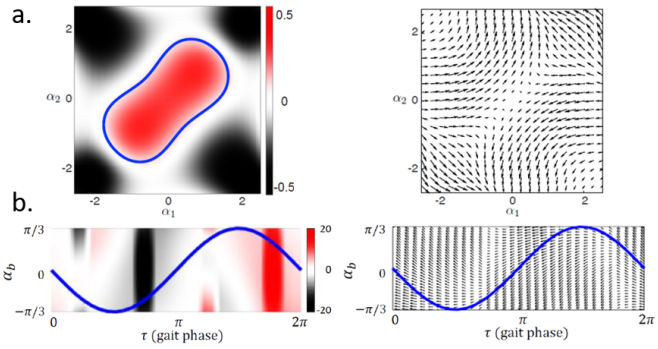

Fig. 2. **Height functions and connection vector fields for two typical systems** (a) height function (left) and connection vector field (right) corresponding to the forward motion of a three-link swimmer in a viscous field [51]. (b) height function (left) and connection vector field (right) corresponding to the forward motion of a quadruped robot on granular surface [1]. Blue curves represent sample gaits

In limbless systems, the shape space $(\mathbb{R}^2)$ is Euclidean, as in Fig. 2(a). The displacement is approximated by the volume enclosed by the gait path. In legged systems, a shape space, like a phase variable, often has a cyclic dimension, so the shape space $(\mathbf{S}^1 \times \mathbf{R}^1)$ can be cylindrical, as in Fig. 2(b). Prior work has shown that the displacement in the area integral (2) is the surface integral below the path [50]. Therefore, the gait design problem in this work is reduced to find a cyclical path in the shape space that maximizes the area below the curve.

[1] the foreright leg is always in phase with the hindleft leg; while foreleft leg is always in phase with the hindright leg

2.3 Dimensionality Reduction

Although [52] have applied geometric tools in more than two dimensions, we choose to use two-dimensional shape spaces so that we can easily visualize height functions. We prescribe the multi-legged locomotion into two shape variables [1].

We now introduce quadruped gait variables, as depicted in Fig. 1(c). A binary *contact state c* describes the contact states, either $c = 0$ (no contact) or $c = 1$ (full contact), and $C = [c_1\ c_2\ c_3\ c_4]^T$ denotes the leg contact states of all four limbs. A set of shape variables contains the body angle α_b and the lateral leg angle set $\beta = [\beta_1\ \beta_2\ \beta_3\ \beta_4]^T$ for four limbs.

We assume that the contact state c and the leg angle β could be parameterized by one periodic variable, gait phase τ, i.e.,

$$c_i = h_i(\tau),\ \beta_i = f_i(\tau),\ i = 1,2,3,4. \tag{4}$$

Therefore, we simplify the quadruped locomotion shape changes into two shape variables: gait phase τ and body angle α. Since τ is periodic but α is not, the shape space is cylindrical.

2.4 Tail-like Appendage

In nature, animals utilize tails to aid in both maneuvering and stabilization. In terms of maneuvering, tails are used by geckos to reorient while jumping [53] and cheetahs to turn during running [54]. In terms of stabilization, tails are used by lizards to keep balance during running [55] and monkeys to aid in climbing [56]. Based on these observations, a number of research groups have attempted to implement tail structures. For example, a robot with a tail can right itself in a fall [53], a cheetah robot proves that the tail can be more effective than reaction wheels in orienting the body when space, power and time are limited [57], and a tail can also stabilize the robot when it is leaping [58]. These tail-like structures have been implemented as single-DoF (degree of freedom) pendulums. Multi-DoF tail research is more limited [59]. Inspired by the work [60] which analyzes how a six DoF serpentine planar robotic tail impacts quadruped's maneuverability in the yaw direction, we are interested in implementing an actuated multi-segment tail which can swing in the pitch direction (Fig. 1(e)) and realizing the tail's swinging in the yaw direction through backbending. With the help of tail, a quadruped can take advantage of the higher stride displacement of the DS gait while maintaining stability.

2.5 Self Manipulation Modeling

Two main approaches have been used to analyze the dynamics of tails: Newton-Euler methods [61] or Lagrangian equations [62, 63]. Among previous work involving tail dynamics, [59, 57, 55, 60] utilized Newton-Euler methods to compute dynamic terms recursively and further implement numerically, especially [60] built a mathematical model of multi-DoF tail but calculations of forces and torques are complicated, making it hard to investigate the dynamic system analytically. Inspired by [64, 54] which developed dynamic equations of tailed system from the Lagrangian and [19] which claimed that using self-manipulation can express a robot's Lagrangian dynamics together with the constraint forces required to sustain them for any combination of legs and other body parts contacting rigid ground as a single "equation of motion", we model our system as a self-manipulator to derive the desired tail motion.

3 Coordinating Backbending to Leg Movements

This section demonstrates how backbending is coordinated to quadruped's leg movements on level ground. Section 3.1 presents how geometric tools are coordinated to leg movements for quadruped on level ground. Section 3.2 shows the results of simulations and robot experiments.

3.1 Geometric Mechanics on Level Ground

Geometric mechanics provides the foundation of the work in this work. In this section, section 3.1.1 illustrates the friction model that allows the application of geometric tools. Section 3.1.2 and Section 3.1.3 presents the designed forward and turning motions. Section 3.1.4 is an additional linearity check to show when analytic derivation is not applicable, numerical computation is a reasonable option to be utilized for geometric tools.

3.1.1 Friction Model

The salamander species we compare against (fire salamander) has its limbs well-developed to lift the body from the ground when locomoting on a flat surface. We therefore design our model and robot so that it has at most four points of contact at the feet, and the mid-section does not drag on the ground. The contacts between the feet and the ground are subjected to Coulomb friction. We observe the walk gait used by the fire salamander is a gait with nearly evenly spaced leg lifting following the sequence foreright, hindleft, foreleft, hindright. Then we assume the surface is frictional enough to prevent feet from slipping and there are no linear velocities on all stance feet. We treat the endpoints of all stance legs as fixed end-effectors.

With the desired configuration of end-effectors and known joint velocities, the Pfaffian constraint can be

$$\begin{bmatrix} 0\\0\\0\\0\\0\\0 \end{bmatrix} = \begin{bmatrix} \dot{x}_1\\ \dot{y}_1\\ \dot{x}_2\\ \dot{y}_2\\ \dot{x}_3\\ \dot{y}_3 \end{bmatrix} = A \begin{bmatrix} \xi\\ \dot{\alpha}\\ \dot{\beta}\\ \dot{\phi}\\ \dot{\varepsilon} \end{bmatrix}, \tag{5}$$

where linear velocities $\dot{x}_1$, $\dot{x}_2$, $\dot{x}_3$ in x direction and $\dot{y}_1$, $\dot{y}_2$, $\dot{y}_3$ in y direction of all stance legs are zero, A represents a set of constraints, containing linearly independent row vectors, $\xi = [\xi_x\ \xi_y\ \xi_\theta]^T$ is the body velocity, α is the body bending angle,

$\beta \in \mathbb{R}^4$ are lateral leg angles, $\phi \in \mathbb{R}^4$ are angles that measures how much each leg is away from the pitch plane of the robot (Fig. 1d), all stance limbs share the same ϕ while the lifting limb has $\phi = 0$. We need to introduce an extra DoF ε on the leg (Fig. 1d), in order to compensate the difference of linear velocities of β. $\dot{\beta}, \dot{\phi}, \dot{\varepsilon}$ are their derivatives representing shape changes, and are able to be parameterized by one periodic variable, gait phase τ.

$$\beta_i = h_i(\tau),\ \phi_i = f_i(\tau),\ \varepsilon_i = e_i(\tau) \tag{6}$$

where $i = 1,2,3,4$ corresponds to foreright, foreleft, hindright and hindleft leg respectively. With $\gamma = [\tau, \alpha]$, given shape velocities $\dot{\gamma}$, we can derive the *kinematic reconstruction equation* from Eq. 5,

$$\xi = A(\gamma)\dot{\gamma}, \tag{7}$$

and $A(\gamma)$ is the new *local connection* mapping shape velocities $\dot{\gamma}$ to body velocities ξ.

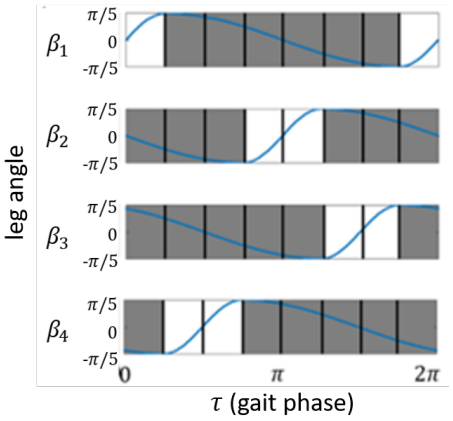

Fig. 3. **Prescribed leg-movement function.** the blue curves as a function of gait phase are listed as the joint angle β and the stance phase c is indicated by the shading.

3.1.2 Forward Motion

We simplify the quadruped locomotion shape changes into two shape variables: gait phase τ and body angle α. Prior work [1] introduced multiple leg movements prescribed by gait phase τ. For the walking gait, the derivation of functions of contact variable c and the leg angle β is shown in Fig. 3.

However, the choice of the path in the shape space (τ, α) is somewhat different from the prior work. The salamander mainly exhibits body undulation in a standing wave with the node at the girdle while walking on the ground, especially when the trunk is lifted [65, 66, 67]. A typical equation for a standing wave is

$$\alpha = a\sin(\omega x)\sin(\omega\tau), \tag{8}$$

where a is the amplitude, ω is the angular frequency, normally equal to 1 here, λ is the wavelength and x is the variable for longitudinal position. In our implementation, body bending joint is anchored around the middle of the body which means $sin(x)$ is a constant. The path can be simplified as

$$\alpha = a\sin(\tau + b), \tag{9}$$

where $a = \frac{\pi}{6}$ due to animal's joint angle limit and b is the phase shift, determined by the gait we choose.

3.1.3 Turning Motion

Real salamanders' turning on ground has not been quantitatively studied yet [1]. There is neither quantified evidence showing the contributions of the limbs to turning nor quantified study about the contributions of the curvature of the trunk to turning [68]. [68] observed that the curvature of the trunk is higher on one side while turning. [42] observed that salamanders use their front legs to step aside to turn.

In this paper, we assume both limbs and backbending play an important role in salamander's turning motion. For example, if the salamander turns right, its limbs can be helpful if lateral leg angle of left-side legs β_2 and β_4 have higher amplitude than lateral leg angle of right-side legs β_1 and β_3. Backbending can contribute to the turning if α has higher amplitude when bending to right side than bending to left side.

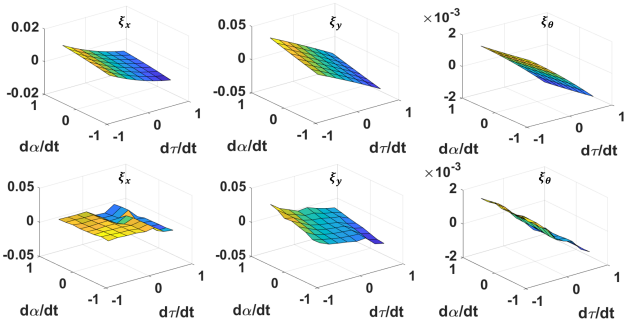

Fig. 4. **Body velocity ξ as functions of shape velocity $\dot{r}$.** (Top) example of *fore leg swinging* with $r = (0.25, -0.35)$ radians. (Bottom) example of *hind leg swinging* with $r = (1.01, -0.17)$ radians. Body velocities are given in terms of the body length (ξ_x and ξ_y) or radians (ξ_θ) per second. Graphs are nearly planar showing that body velocity is linearly proportional to shape velocity.

3.1.4 Numerical Computation of the *Local Connection* and Linearity Check

The key assumption in applying geometric theory to kinematic locomotion study is that at any given shape, the robot's body velocity is linearly proportional to its shape velocity [69]. In a multi-legged system, the non-linearity of

Coulomb friction restricts the analytic derivation of such linearity and therefore the analytic derivation of the *local connection* is not applicable. Our friction model formulates the connection between body velocities and shape changes from velocity constraints of the system and allows us to identify the *local connection* (see Section 2.2) numerically as developed by [51]. The *local connection* of a quadrupedal robot locomoting on level ground can be approximated by numerically measuring displacements in the body frame. It then can be used to plot height functions.

In this study, inspired by [69], we provide an additional linearity check to show that such numerical means can derive the linear mapping from shape velocity to body velocity. With our friction models, graphs of body velocity ξ as functions of shape velocity $\dot{r}$ are nearly planar across the shape space, as displayed in Fig. 4.

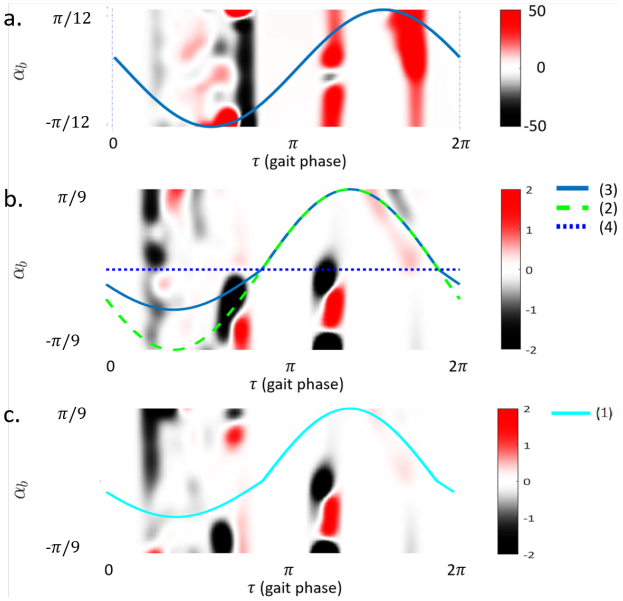

Fig. 5. **(a) Forward motion height function (ξ_x). (b) Rotational height function (ξ_θ) of even leg amplitudes. (c) Rotational height function (ξ_θ) of uneven leg amplitudes.** (a) Height function is computed for the leg movement in Fig. 3. (b)(c) The gait path with the most maximum volume (best gait) underneath is the gait with the largest turning angle per gait cycle. Comparing (b) and (c) shows that using uneven leg amplitude contributes more to turning. From (c), the combination of uneven leg amplitude and even bending amplitude (2) produces maximum turning angle.

3.2 Experiments

Taking a robophysical approach [12], we built a salamander robot to test its performance on level ground. This robot (1255g, ∼28cm), as shown in Fig. 1bcd, is open-loop and servo-driven. Each leg has three servo motors to control its vertical position and step size. The body has one servo motor in the middle to adjust the body angle and two servos on the head and hip respectively to serve as fixed joints. The frame of the body is 3D-printed.

In our experiment, the robot executed programmed gaits on the rubber mat. During each experiment, the robot's starting and final head and COM positions are identified. The ratio of the net displacement per gait cycle to the body length is measured for the forward motion and the turning angle is measured for the turning motion as well. Four trials were taken for each motion.

3.2.1 Forward Motion

When moving forward, we assume a keeps constant and is set to be $\frac{\pi}{12}$ which matches the tracked data from the salamander. We compute the forward height function (Fig. 5a) and recall that for height functions on cylinders, the net displacement of the gait is the volume underneath the gait path. The gait path with the most maximum volume (best gait) is the gait with the largest forward stride displacement per gait cycle. The blue curve in the Fig. 5a is the best gait path.

We verify our gaits with friction force model simulation and robot experiments on the rubber mat (Fig. 6ac). Both suggest that the proper body-limb coordination can improve the stride displacement. In the simulation, the net displacement per gait cycle with backbending is improved by 17.71% compared to the movement without backbending and the average net displacement for the robot increases by 18.03%.

3.2.2 Turning Motion

To find out whether limbs, backbending or both contribute to the turning motion and how much do they contribute, we take right-turning as an example and compare four different limb and bodybending combinations:

1. even leg amplitude ($\beta \in [-\pi/5, \pi/5]$) with uneven body amplitude ($\alpha \in [-\pi/18, \pi/9]$);
2. uneven leg amplitude ($\beta_{2,4} \in [-\pi/5, \pi/5], \beta_{1,2} \in [-\pi/7, \pi/7]$) with even body amplitude ($\alpha \in [-\pi/9, \pi/9]$);
3. uneven leg amplitude and uneven body amplitude;
4. uneven leg amplitude and zero body-bending.

Height functions and sample gaits are shown in Fig. 5. The net right-turning angle of the gait is the volume underneath the gait path. The gait path with the most maximum volume produces the largest turning angle per gait cycle. Combination (2) leads to the maximum right-turning, followed by (3), while (1) and (4) are not helpful in turning. Our results are verified by friction force model simulation and robot test. As displayed in Fig. 6b, the combination of uneven leg amplitude and uneven body bending leads to the largest turning angle. We can assume that uneven lateral leg amplitude plays an important role in turning behavior, while uneven body-bending amplitude is much more helpful when combined with uneven leg amplitude.

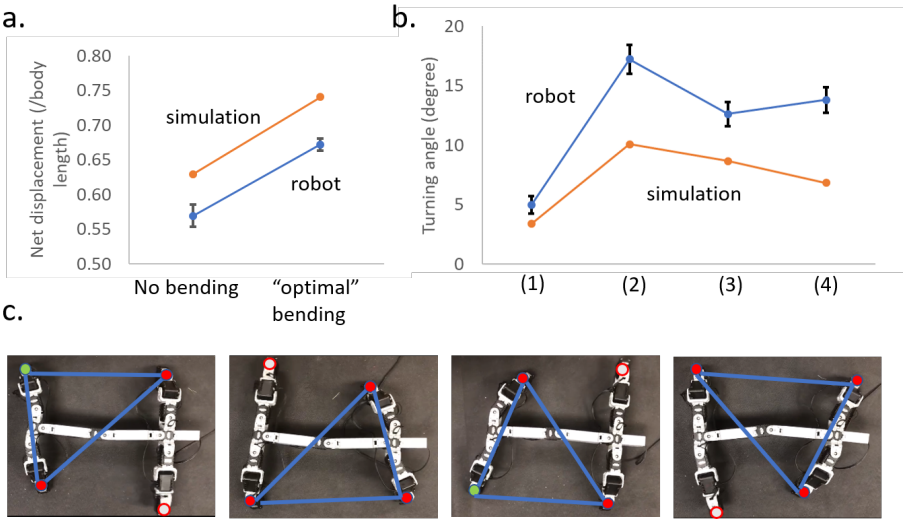

Fig. 6. **Experiment results and set-ups** (a) Comparison of the model with robot experiments in forward walk motion: the net displacement in terms of body length of the model/robot with no-bending and "best-bending". (b) Comparison of the model with robot experiments in turning walk motion: the turning angle of model/robot with combination (1), (2), (3) and (4). (c) Sequence of snapshots of robot's forward walk gait. The red dot represents the stance leg without slip. The green dot represents the stance leg with slip. The white dot represents the swinging leg. The blue lines represent the supporting polygon.

4 Inertia Tail-like Appendage

4.1 LS and DS Gaits

In both LS and DS gaits, all legs have the same duty factor, and the only difference lies in the sequence under which the foot is lifted off the ground: the LS gait has the footfall sequence of foreright-hindleft-foreleft-hindright while the DS gait has the sequence of foreright-hindright-foreleft-hindleft. Following the Hildebrand diagram [18], we numerically measured the stride displacement and stability of walking gaits with different duty factors (% of stride that each foot is on the ground) and leg phase shifts (% of stride that fore footfall follows hind on same side). We projected the stride displacement and stability heat maps onto the Hildebrand diagram, as shown in Fig. 7 8, which show that, under the same duty factor, the DS gait always has higher stride displacement than LS gait but is less stable.

4.2 Self-Motion

We aimed to use a tail-like appendage to stabilize the DS gait in order to achieve a higher-speed as well as a stable gait. Meanwhile, we also believe backbending can not only increase the motion speed but also help the tail stabilize the gait.

With a tail, the center of mass (COM) of the system shifts outside the supporting polygon only when hind legs are lifted. At each moment of a gait, stance leg angles $\beta = [\beta_1\ \beta_2\ \beta_3]$ and their derivatives are known. The changes of other two DoFs of each stance leg are negligible and the second segment of each leg, like B_1C_1, can be regarded as perpendicular to the ground.

We modeled the system as a self manipulator in 3D [19]. The quadruped body has three leg links (Fig. 9) touching the ground and a tail link (Fig. 10) swinging in the air. $\theta = [\theta_1\ \theta_2\ \theta_3\ \theta_4]$ are tail joint angles in the xz plane, $\xi = [o_x\ o_y\ o_z\ o_\alpha\ o_\beta\ o_\varphi]^T \in \mathrm{R}^6$ are object orientations. The model parameters contain $r = [\alpha\ \theta\ \beta\ \varepsilon]^T \in \mathrm{R}^{13}$ and ξ. We define J^b_{pj} as the jth element of final body manipulator Jacobian, where j can refer to either tail links or leg links, similar in M_j, g_{pj} and $\mathrm{Ad}_{g_{pj}}$.

The Euler-Lagrange equation can be derived and expressed in the form

$$M(r,\xi)\begin{bmatrix}\ddot{r}\\ \ddot{\xi}\end{bmatrix} + C\begin{bmatrix}\dot{r}\\ \dot{\xi}\end{bmatrix} + N + A^T\lambda = \Upsilon, \tag{10}$$

where the manipulator inertia matrix is

$$M = \begin{bmatrix} Id & \\ & J^{b^T}_{op}\end{bmatrix}\hat{M}\begin{bmatrix} Id & \\ & J^{b}_{op}\end{bmatrix}, \tag{11}$$

$$\hat{M} = \begin{bmatrix} \sum J^{b^T}_{pj} M_j J^b_{pj} & \sum J^{b^T}_{pj} M_j \mathrm{Ad}_{g^{-1}_{pj}} \\ \sum \mathrm{Ad}^T_{g^{-1}_{pj}} M_j J^b_{pj} & M_o + \sum \mathrm{Ad}^T_{g^{-1}_{pj}} M_j \mathrm{Ad}_{g^{-1}_{pj}}\end{bmatrix}, \tag{12}$$

the Coriolis matrix is

$$C_{ij} = \frac{1}{2}\sum_k \left(\frac{\partial M_{ij}}{\partial q_k} + \frac{\partial M_{ik}}{\partial q_j} - \frac{\partial M_{kj}}{\partial q_i}\right)\dot{q}_k, \tag{13}$$

N comes from the gravitational potential energy, and $A =$

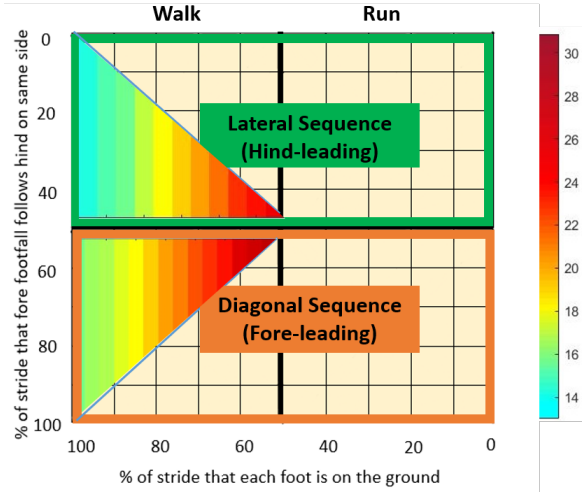

Fig. 7. **Stride Displacement Projected on Hildebrand Diagram** The x axis is the duty factor, the y axis is the leg phase shift. The color bar shows more red in color map, more stride displacement the gait produces. Under same duty factor, DS gait has higher stride displacement than LS gait.

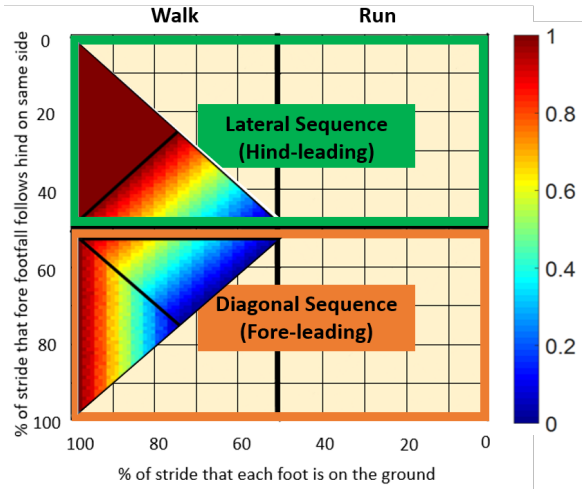

Fig. 8. **Stability Heat Map Projected on Hildebrand Diagram** The x axis is the duty factor, the y axis is the leg phase shift. The color bar shows more red in color map, more stable the gait is. Under same duty factor, DS gait is less stable than LS gait.

$\begin{bmatrix}0\,0\,0\,0\,0 & -J_h\,\bar{G}_s^T\end{bmatrix}^T$ where

$$J_h = \text{diag}(0,\ \ldots\ 0,\ B_{c_1}^T \text{Ad}_{g_{s_1c_1}^{-1}} J_{s_1f_1}^s, \ldots\ B_{c_3}^T \text{Ad}_{g_{s_3c_3}^{-1}} J_{s_3f_3}^s), \tag{14}$$

$$\bar{G}_s^T = \begin{bmatrix}\text{Ad}_{g_{oc_1}^{-1}}^T B_{c_1} & \text{Ad}_{g_{oc_2}^{-1}}^T B_{c_2} & \text{Ad}_{g_{oc_3}^{-1}}^T B_{c_3}\end{bmatrix}^T J_{op}^b, \tag{15}$$

Υ contains desired tail joint torques τ while the rest is assumed to be 0. In order to prevent the robot from falling over, the dynamic equation (10) is required to make sure that λs related to legs in z direction are larger than 0.

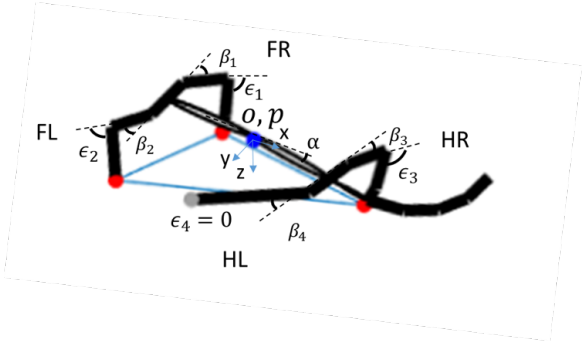

Fig. 9. **Leg model and parameters** $\beta_i (i = 1:4)$ is the leg shoulder angle, $\varepsilon_i (i = 1:4)$ is the leg knee angle, α is the body bending angle.

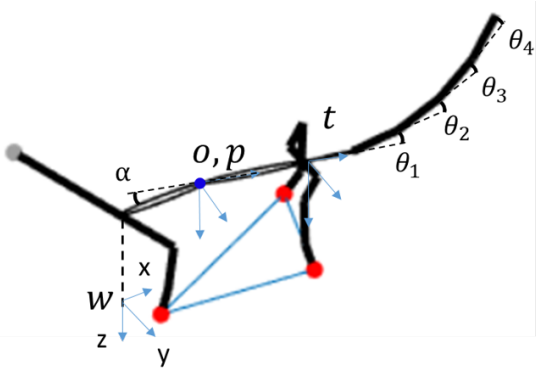

Fig. 10. **Tail model** w is the world frame, followed by the object frame o, p is the quadruped body frame COM, coincident with o, and t is the tail base frame. $\theta_i (i = 1:4)$ is the tail joint angle.

4.3 Implementation

Up to now, the implementation does not work well as expected, mainly because the system contains 19 parameters: r and ξ. When importing the data into the MATLAB function, the manipulator inertia matrix is always nearly singular and its inverse matrix goes to infinity. We have tried to add some noise into the matrix in order to avoid singularity but the result is still too large to make sense. We plan to reduce the dimension in the existing model to see if the problem can be solved.

5 Conclusion

5.1 Body-limb coordination

This work intends to address that, on a level surface, proper body-limb coordination could not only "optimize" the stride displacement in the forward motion, but also have a crucial effect on turning behavior. Both have been verified by our friction model simulation and robot experiments.

We plan to set up further animal experiments to allow salamanders to complete a series of forward and turning motions. We hope to quantitatively study how body-limb coordination contributes to animal's locomotion. Our future work will also include body-limb coordination analysis on other common gaits (like side-stepping turning gait [42] and dynamic trot gait) along with a systematical study of animal's

whole-body coordination based on the evaluation of speed, stability and cost of transport.

5.2 Geometric techniques

We apply and extend geometric techniques to coordinate backbending with prescribed leg movements for quadrupedal locomotion on level ground. It allows us to intuitively and visualizably analyze and design gait paths for various legged-system locomotion behavior. Compared to the feedback control algorithm in CPG, our gait design algorithms do not require prior knowledge of gait shapes. Moreover, we can use our algorithm to generate and optimize the gait trajectories, which could be tracked online to serve as a base of CPG-based approaches.

Geometric tools and coordination methods in this paper could also extend to other bendings which can be represented by a modal function as well as other morphologies which are benefiting from backbending.

5.3 Inertia Tail-like Appendage

With an actuated tail, the back-bending quadruped can walk in DS gait for higher stride displacement while maintaining stability. We want to model the system as a self-manipulator and use a systematic Lagrangian equation to find the appropriate tail motion. However, there still exist some problems in the implementation.

If problems are solved, we will look forward to extend the idea to quadrupedal locomotion on rough terrains or uphill climbing. Moreover, instead of walking gaits, further work could be using the tail to balance dynamic quadrupedal trot gaits.

References

[1] Zhong, B., Aydin, Y. O., Gong, C., Sartoretti, G., Wu, Y., Rieser, J., Xing, H., Rankin, J., Michel, K., Nicieza, A., et al. "Coordination of back bending and leg movements for quadrupedal locomotion". 1, 2, 3, 4

[2] Smit, T. H., 2002. "The use of a quadruped as an in vivo model for the study of the spine-biomechanical considerations". *European Spine Journal,* **11**(2), pp. 137–144. 1

[3] Leeser, K. F., 1996. "Locomotion experiments on a planar quadruped robot with articulated spine". PhD thesis, Massachusetts Institute of Technology. 1

[4] Eckert, P., Spröwitz, A., Witte, H., and Ijspeert, A. J., 2015. "Comparing the effect of different spine and leg designs for a small bounding quadruped robot". In Robotics and Automation (ICRA), 2015 IEEE International Conference on, IEEE, pp. 3128–3133. 1

[5] Crespi, A., Karakasiliotis, K., Guignard, A., and Ijspeert, A. J., 2013. "Salamandra Robotica II: An Amphibious Robot to Study Salamander-Like Swimming and Walking Gaits". *IEEE Transactions on Robotics,* **29**(2), April, pp. 308–320. 1, 2

[6] Marsden, J. E., and Ratiu, T. S., 2013. *Introduction to mechanics and symmetry: a basic exposition of classical mechanical systems*, Vol. 17. Springer Science & Business Media. 1, 2

[7] Marsden, J. E., 1997. "Geometric foundations of motion and control". In Motion, Control, and Geometry: Proceedings of a Symposium, Board on Mathematical Science, National Research Council Education, National Academies Press, Washington, DC. 1, 2

[8] Shapere, A., and Wilczek, F., 1989. "Geometry of self-propulsion at low Reynolds number". *Journal of Fluid Mechanics,* **198**, pp. 557–585. 1, 2

[9] Wilczek, F., and Shapere, A., 1989. *Geometric phases in physics*, Vol. 5. World Scientific. 1, 2

[10] Hatton, R. L., and Choset, H., 2011. "Geometric motion planning: The local connection, Stokes theorem, and the importance of coordinate choice". *The International Journal of Robotics Research,* **30**(8), pp. 988–1014. 1, 2

[11] Shammas, E. A., Choset, H., and Rizzi, A. A., 2007. "Geometric motion planning analysis for two classes of underactuated mechanical systems". *The International Journal of Robotics Research,* **26**(10), pp. 1043–1073. 1, 2

[12] Aguilar, J., Zhang, T., Qian, F., Kingsbury, M., McInroe, B., Mazouchova, N., Li, C., Maladen, R., Gong, C., Travers, M., et al., 2016. "A review on locomotion robophysics: the study of movement at the intersection of robotics, soft matter and dynamical systems". *Reports on Progress in Physics,* **79**(11), p. 110001. 1, 2, 5

[13] Batterman, R. W., 2003. "Falling cats, parallel parking, and polarized light". *Studies in History and Philosophy of Science Part B: Studies in History and Philosophy of Modern Physics,* **34**(4), pp. 527–557. 1, 2

[14] Kelly, S. D., and Murray, R. M., 1995. "Geometric phases and robotic locomotion". *Journal of Field Robotics,* **12**(6), pp. 417–431. 1, 2

[15] Ostrowski, J., and Burdick, J., 1998. "The geometric mechanics of undulatory robotic locomotion". *The international journal of robotics research,* **17**(7), pp. 683–701. 1, 2

[16] McInroe, B., Astley, H. C., Gong, C., Kawano, S. M., Schiebel, P. E., Rieser, J. M., Choset, H., Blob, R. W., and Goldman, D. I., 2016. "Tail use improves performance on soft substrates in models of early vertebrate land locomotors". *Science,* **353**(6295), pp. 154–158. 1

[17] Aydin, Y. O., Chong, B., Gong, C., Rieser, J. M., Rankin, J. W., Michel, K., Nicieza, A. G., Hutchinson, J., Choset, H., and Goldman, D. I., 2017. "Geometric Mechanics Applied to Tetrapod Locomotion on Granular Media". In Conference on Biomimetic and Biohybrid Systems, Springer, pp. 595–603. 1

[18] Hildebrand, M., 1965. "Symmetrical gaits of horses". *science,* **150**(3697), pp. 701–708. 1, 6

[19] Johnson, A. M., and Koditschek, D. E., 2013. "Legged self-manipulation". *IEEE Access,* **1**, pp. 310–334. 1, 3, 6

[20] Kolter, J. Z., Rodgers, M. P., and Ng, A. Y., 2008. "A control architecture for quadruped locomotion over

rough terrain". In Robotics and Automation, 2008. ICRA 2008. IEEE International Conference on, IEEE, pp. 811–818. 1

[21] Zucker, M., Ratliff, N., Stolle, M., Chestnutt, J., Bagnell, J. A., Atkeson, C. G., and Kuffner, J., 2011. "Optimization and learning for rough terrain legged locomotion". *The International Journal of Robotics Research,* **30**(2), pp. 175–191. 1

[22] Mcghee, R. B., and Iswandhi, G. I., 1979. "Adaptive Locomotion of a Multilegged Robot over Rough Terrain". *IEEE Transactions on Systems, Man, and Cybernetics,* **9**(4), April, pp. 176–182. 1

[23] Bai, S., Low, K. H., Seet, G., and Zielinska, T., 1999. "A new free gait generation for quadrupeds based on primary/secondary gait". In Proceedings 1999 IEEE International Conference on Robotics and Automation (Cat. No.99CH36288C), Vol. 2, pp. 1371–1376 vol.2. 1

[24] Kim, M. S., and Uther, W., 2003. "Automatic Gait Optimisation for Quadruped Robots". In In Australasian Conference on Robotics and Automation. 1

[25] Powell, M. J., 1964. "An efficient method for finding the minimum of a function of several variables without calculating derivatives". *The computer journal,* **7**(2), pp. 155–162. 1

[26] Kohl, N., and Stone, P., 2004. "Policy gradient reinforcement learning for fast quadrupedal locomotion". In Robotics and Automation, 2004. Proceedings. ICRA '04. 2004 IEEE International Conference on, Vol. 3, pp. 2619–2624 Vol.3. 1

[27] Stone, P., Dresner, K., Erdogan, S. T., Fidelman, P., Jong, N. K., Kohl, N., Kuhlmann, G., Lin, E., Sridharan, M., Stronger, D., et al., 2003. "UT Austin Villa 2003: A new RoboCup four-legged team". 1

[28] Chernova, S., and Veloso, M., 2004. "An evolutionary approach to gait learning for four-legged robots". In 2004 IEEE/RSJ International Conference on Intelligent Robots and Systems (IROS) (IEEE Cat. No.04CH37566), Vol. 3, pp. 2562–2567 vol.3. 1

[29] Delvolve, I., Branchereau, P., Dubuc, R., and Cabelguen, J.-M., 1999. "Fictive rhythmic motor patterns induced by NMDA in an in vitro brain stemspinal cord preparation from an adult urodele". *Journal of Neurophysiology,* **82**(2), pp. 1074–1077. 1, 2

[30] Saranli, U., Buehler, M., and Koditschek, D. E., 2001. "RHex: A Simple and Highly Mobile Hexapod Robot". *The International Journal of Robotics Research,* **20**(7), pp. 616–631. 2

[31] Buehler, M., Battaglia, R., Cocosco, A., Hawker, G., Sarkis, J., and Yamazaki, K., 1998. "SCOUT: A simple quadruped that walks, climbs, and runs". In Robotics and Automation, 1998. Proceedings. 1998 IEEE International Conference on, Vol. 2, IEEE, pp. 1707–1712. 2

[32] Buehler, M., Cocosco, A., Yamazaki, K., and Battaglia, R., 1999. "Stable open loop walking in quadruped robots with stick legs". In Robotics and Automation, 1999. Proceedings. 1999 IEEE International Conference on, Vol. 3, IEEE, pp. 2348–2353. 2

[33] Altendorfer, R., Moore, N., Komsuoglu, H., Buehler, M., Brown, H., McMordie, D., Saranli, U., Full, R., and Koditschek, D., 2001. "RHex: A Biologically Inspired Hexapod Runner". *Autonomous Robots,* **11**(3), Nov, pp. 207–213. 2

[34] Cham, J. G., Karpick, J. K., and Cutkosky, M. R., 2004. "Stride Period Adaptation of a Biomimetic Running Hexapod". *The International Journal of Robotics Research,* **23**(2), pp. 141–153. 2

[35] Alexander, R. M., 1984. "The Gaits of Bipedal and Quadrupedal Animals". *The International Journal of Robotics Research,* **3**(2), pp. 49–59. 2

[36] Smith, J. A., and Poulakakis, I., 2004. "Rotary gallop in the untethered quadrupedal robot scout II". In 2004 IEEE/RSJ International Conference on Intelligent Robots and Systems (IROS) (IEEE Cat. No.04CH37566), Vol. 3, pp. 2556–2561 vol.3. 2

[37] Wheatley, M., Jovanovic, K., Stein, R. B., and Lawson, V., 1994. "The activity of interneurons during locomotion in the in vitro necturus spinal cord". *Journal of Neurophysiology,* **71**(6), pp. 2025–2032. 2

[38] Owaki, D., Kano, T., Nagasawa, K., Tero, A., and Ishiguro, A., 2013. "Simple robot suggests physical interlimb communication is essential for quadruped walking". *Journal of The Royal Society Interface,* **10**(78). 2

[39] Ijspeert, A. J., Crespi, A., Ryczko, D., and Cabelguen, J.-M., 2007. "From Swimming to Walking with a Salamander Robot Driven by a Spinal Cord Model". *Science,* **315**(5817), pp. 1416–1420. 2

[40] Cruse, H., 1990. "What mechanisms coordinate leg movement in walking arthropods?". *Trends in Neurosciences,* **13**(1), pp. 15 – 21. 2

[41] Ijspeert, A. J., 2001. "A connectionist central pattern generator for the aquatic and terrestrial gaits of a simulated salamander". *Biological Cybernetics,* **84**(5), Apr, pp. 331–348. 2

[42] Harischandra, N., Cabelguen, J.-M., and Ekeberg, Ö., 2010. "A 3D musculo-mechanical model of the salamander for the study of different gaits and modes of locomotion". *Frontiers in neurorobotics,* **4**, p. 112. 2, 4, 7

[43] Zhou, D., and Low, K., 1999. "A friction constraint method for the force distribution of Quadruped Robots". In Advanced Intelligent Mechatronics, 1999. Proceedings. 1999 IEEE/ASME International Conference on, IEEE, pp. 866–871. 2

[44] Liu, H., and Wen, B., 1997. "Force distribution for the legs of a quadruped walking vehicle". *Journal of Robotic Systems,* **14**(1), pp. 1–8. 2

[45] Tarokh, M., and Lee, M., 2008. "Kinematics modeling of multi-legged robots walking on rough terrain". In 2008 Second International Conference on Future Generation Communication and Networking Symposia, IEEE, pp. 12–16. 2

[46] Chen, X., Watanabe, K., Kiguchi, K., and Izumi, K., 1999. "Optimal force distribution for the legs of a

quadruped robot". *Machine Intelligence and Robotic Control,* **1**(2), pp. 87–93. 2

[47] Buchli, J., Kalakrishnan, M., Mistry, M., Pastor, P., and Schaal, S., 2009. "Compliant quadruped locomotion over rough terrain". In Intelligent Robots and Systems, 2009. IROS 2009. IEEE/RSJ International Conference on, IEEE, pp. 814–820. 2

[48] Pongas, D., Mistry, M., and Schaal, S., 2007. "A robust quadruped walking gait for traversing rough terrain". In Robotics and Automation, 2007 IEEE International Conference on, IEEE, pp. 1474–1479. 2

[49] Dai, J., Faraji, H., Gong, C., Hatton, R. L., Goldman, D. I., and Choset, H., 2016. "Geometric Swimming on a Granular Surface.". In Robotics: Science and Systems. 2

[50] Gong, C., Whitman, J., Grover, J., Chong, B., Ren, R., and Choset, H., 2018. "Geometric motion planning for systems with toroidal and cylindrical shape spaces (accepted)". In ASME Dynamic Systems and Control Conference (DSCC). 2

[51] Gong, C., Goldman, D. I., and Choset, H., 2016. "Simplifying Gait Design via Shape Basis Optimization.". In Robotics: Science and Systems. 2, 5

[52] Ramasamy, S., and Hatton, R. L., 2017. "Geometric gait optimization beyond two dimensions". In American Control Conference (ACC), 2017, IEEE, pp. 642–648. 3

[53] Chang-Siu, E., Libby, T., Tomizuka, M., and Full, R. J., 2011. "A lizard-inspired active tail enables rapid maneuvers and dynamic stabilization in a terrestrial robot". In Intelligent Robots and Systems (IROS), 2011 IEEE/RSJ International Conference on, IEEE, pp. 1887–1894. 3

[54] Patel, A., and Boje, E., 2015. "On the conical motion of a two-degree-of-freedom tail inspired by the cheetah". *IEEE Transactions on Robotics,* **31**(6), pp. 1555–1560. 3

[55] Park, H. S., Floyd, S., and Sitti, M., 2009. "Dynamic modeling and analysis of pitch motion of a basilisk lizard inspired quadruped robot running on water". In 2009 IEEE International Conference on Robotics and Automation, IEEE, pp. 2655–2660. 3

[56] Li, W.-Y., Wang, Y.-H., Kuo, C.-T., and Lin, P.-C., 2017. "Design and implementation of a spider monkey robot". In 2017 International Conference on Advanced Robotics and Intelligent Systems (ARIS), IEEE, pp. 62–62. 3

[57] Briggs, R., Lee, J., Haberland, M., and Kim, S., 2012. "Tails in biomimetic design: Analysis, simulation, and experiment". In 2012 IEEE/RSJ International Conference on Intelligent Robots and Systems, IEEE, pp. 1473–1480. 3

[58] Brill, A., De, A., Johnson, A., and Koditschek, D., 2015. "Tail-assisted rigid and compliant legged leaping". 3

[59] Mutka, A., Orsag, M., and Kovacic, Z., 2013. "Stabilizing a quadruped robot locomotion using a two degree of freedom tail". In 21st Mediterranean Conference on Control and Automation, IEEE, pp. 1336–1342. 3

[60] Rone, W., and Ben-Tzvi, P., 2016. "Dynamic modeling and simulation of a yaw-angle quadruped maneuvering with a planar robotic tail". *Journal of Dynamic Systems, Measurement, and Control,* **138**(8), p. 084502. 3

[61] Bennani, M., and Giri, F., 1996. "Dynamic modelling of a four-legged robot". *Journal of Intelligent and Robotic Systems,* **17**(4), pp. 419–428. 3

[62] Perrin, B., Chevallereau, C., and Verdier, C., 1997. "Calculation of the direct dynamic model of walking robots: Comparison between two methods". In Proceedings of International Conference on Robotics and Automation, Vol. 2, IEEE, pp. 1088–1093. 3

[63] Zamani, A., Khorram, M., and Moosavian, S. A. A., 2011. "Dynamics and stable gait planning of a quadruped robot". In 2011 11th International Conference on Control, Automation and Systems, IEEE, pp. 25–30. 3

[64] Shamsah, A., De, A., and Koditschek, D. E., 2018. "Analytically-guided design of a tailed bipedal hopping robot". In 2018 IEEE/RSJ International Conference on Intelligent Robots and Systems (IROS), IEEE, pp. 2237–2244. 3

[65] Frolich, L. M., and Biewener, A. A., 1992. "Kinematic and electromyographic analysis of the functional role of the body axis during terrestrial and aquatic locomotion in the salamander Ambystoma tigrinum". *Journal of Experimental Biology,* **162**(1), pp. 107–130. 4

[66] Delvolvé, I., Bem, T., and Cabelguen, J.-M., 1997. "Epaxial and limb muscle activity during swimming and terrestrial stepping in the adult newt, Pleurodeles waltl". *Journal of Neurophysiology,* **78**(2), pp. 638–650. 4

[67] Ashley-Ross, M. A., and Bechtel, B. F., 2004. "Kinematics of the transition between aquatic and terrestrial locomotion in the newt Taricha torosa". *Journal of Experimental Biology,* **207**(3), pp. 461–474. 4

[68] Crespi, A., Karakasiliotis, K., Guignard, A., and Ijspeert, A. J., 2013. "Salamandra robotica II: an amphibious robot to study salamander-like swimming and walking gaits". *IEEE Transactions on Robotics,* **29**(2), pp. 308–320. 4

[69] Hatton, R. L., Ding, Y., Choset, H., and Goldman, D. I., 2013. "Geometric visualization of self-propulsion in a complex medium". *Physical review letters,* **110**(7), p. 078101. 4, 5